Electric quadrupole moments and isotope shifts of radioactive sodium isotopes

F. Touchard, J. M. Serre, S. Büttgenbach,* P. Guimbal, R. Klapisch,† M. de Saint Simon, and C. Thibault
Laboratoire René Bernas
du Centre de Spectrométrie Nucleaire et de Spectrométrie de Masse,
Bât. 108, 91406 Orsay, France

H. T. Duong, P. Juncar, S. Liberman, J. Pinard, and J. L. Vialle
Laboratoire Aimé Cotton,‡ Centre National de la Recherche Scientifique II, Bât. 505, 91405 Orsay, France
(Received 28 December 1981)

On-line high resolution laser spectroscopy has been performed on radioactive $^{20-31}$Na. New values for the isotope shift of the D_1 line of $^{20-24,31}$Na relative to ^{23}Na have been obtained. The spectroscopic quadrupole moments of $^{21,25-29}$Na have been determined using a double resonance method. The D_2 line hyperfine structure of $^{21,25-27}$Na has also been studied by laser optical spectroscopy. Results are in agreement with those obtained by rf double resonance. No evidence of the sudden onset of a deformation expected at $N=20$ has been found. A strong shell effect in the change in the mean-square charge radius is exhibited at $N=14$.

[NUCLEAR REACTIONS $^{20-24,31}$Na; measured isotope shift. $^{20-22,24,31}$Na; measured hyperfine constants $A(3s\ ^2S_{1/2})$, $A(3p\ ^2P_{1/2})$; deduced μ. $^{21,25-29}$Na; measured hyperfine constants $A(3p\ ^2P_{3/2})$, $B(3p\ ^2P_{3/2})$; deduced Q. Atomic beam laser spectroscopy and laser rf double-resonance spectrosopy.]

I. INTRODUCTION

In previous experiments,[1,2] we studied the hyperfine structure (hfs) and the isotope shift (IS) of the D_1 line of $^{21-31}$Na. Nuclear properties (spins I, magnetic moments μ_I, and changes in the mean square charge radius $\delta\langle r^2\rangle^{A,A'}$) were deduced from these experiments. However, if the hfs of the D_2 line could be studied, the electric quadrupole moment could be deduced from the hyperfine B constant of the $^2P_{3/2}$ excited state, and therefore additional information on the nuclear deformation would be gained. In particular, it could be interesting to study the quadrupole moments of nuclei around $N=20$, since two neutron binding energy systematics,[3] Hartree-Fock calculations,[4] and energy systematics of the first 2^+ level in even-A magnesium isotopes[5] seem to indicate a sudden deformation occurring at $N=20$. Unfortunately, in the case of sodium isotopes, the hyperfine intervals of the $3p\ ^2P_{3/2}$ state are comparable to the residual Doppler broadening usually obtained in our apparatus,[1,2,6] so that the hyperfine components are not completely resolved. Moreover, the B factors are expected to be small so that very precise measurements of the hyperfine intervals (to an accuracy of the order of 1 MHz) are needed. For these reasons, the results we have obtained in previous attempts[1,6] are not very accurate and must be considered with care.

In order to perform more reliable measurements and to extend them to other less abundant radioactive isotopes, we have developed two different experimental techniques which have been used concurrently.

First, the apparatus has been modified to reduce the Doppler broadening and to increase the production rates. These modifications, together with a more reliable laser frequency control, allow us to redo the laser optical spectroscopy experiments on the D_2 line of an extended range of isotopes with a higher accuracy and a higher level of confidence. Using the same equipment some additional results on the D_1 line have also been obtained and are reported too.

In addition, we have adapted the double resonance spectroscopy method[7] to our case. This has enabled us to measure very precisely the hyperfine interval ($F'=I+\frac{3}{2}$, $F'=I+\frac{1}{2}$) of the $3p\ ^2P_{3/2}$ atomic state for $^{21,25-29}$Na isotopes. The results obtained are compared to those obtained by laser spectroscopy.

In the following section, we shall describe the apparatus used for the optical spectroscopy. Section

III will deal with the double-resonance experiment, and Sec. IV will be devoted to the discussion of the results.

II. THE OPTICAL EXPERIMENT

The principle of the optical experiment has been described in previous papers.[1,2,8] It rests upon a magnetic detection of optical resonance through the hyperfine or Zeeman optical pumping which is induced by the light of a continuous wave (cw) single-mode tunable dye laser interacting at 90° with a thermal atomic beam [Fig. 1(a)]. In the case of the D_2 line, the "c" transition [Fig. 1(b)] does not induce hyperfine optical pumping. Using a $\sigma^{\pm}$ polarized radiation in the presence of a small static magnetic field H_0, parallel to the laser beam it is possible to induce Zeeman optical pumping between the magnetic sublevels of the $F=I+\frac{1}{2}$ level of the ground state. A change in the m_J value (in a strong magnetic field) may occur and the transition can therefore be detected as a negative signal with σ^- light or a small positive signal with σ^+ light (cf. Ref. 8).

The description of the apparatus is given in the above quoted papers. We shall give here indications concerning only the modified devices. The aim of these modifications is to increase the production of radioactive species and to have a smaller width of the observed resonance peaks. In a first subsection, we shall describe the targets. Then we shall examine the improvements in the resolution of the detected resonances and in the laser frequency control. Finally, we discuss the detection of the atoms and the data processing which will be given together with the results.

A. Production of the atomic beam

Fragmentation reactions are well known to be adequate to produce neutron-rich light nuclei. Several types of targets have been used. After

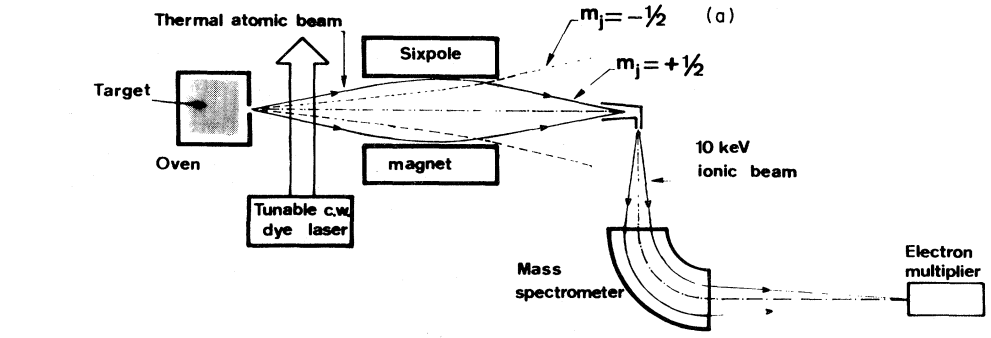

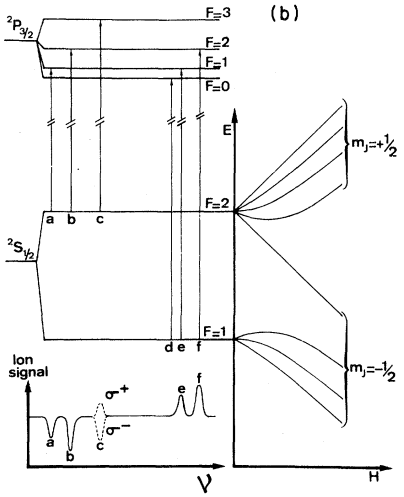

FIG. 1. (a) After impact of the proton beam on the target, the produced isotopes emerge from the oven as a thermal atomic beam which is illuminated by a cw dye laser light. The induced optical pumping produces a change in the relative populations of the two hyperfine levels of the atomic ground state. Moving into the strong inhomogeneous magnetic field of a sixpole magnet, atoms with $m_J=+\frac{1}{2}$ are focused, while atoms with $m_J=-\frac{1}{2}$ are defocused. Alkali atoms are selectively ionized in a L-shaped rhenium device. A mass spectrometer ensures the isotopic selection. An electron multiplier allows counting the selected ions individually. (b) Signals obtained for the D_2 line in the case of $I=\frac{3}{2}$.

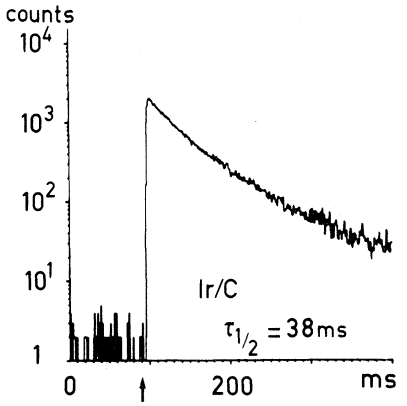

FIG. 2. Diffusion curve of ^{25}Na from the iridium/graphite target. The arrow indicates the passage of the pulsed proton beam. Half of the production is released after 38 ms.

several attempts, we finally adopted a target made of iridium and graphite powders.[9] Diffusion curve and production rates are given in Figs. 2 and 3. In order to study the neutron-deficient isotopes, we used a target made of silicon evaporated on graphite slabs from which $^{20-25}$Na isotopes were produced with rather high rates (Fig. 3).[9] Reference 9 also

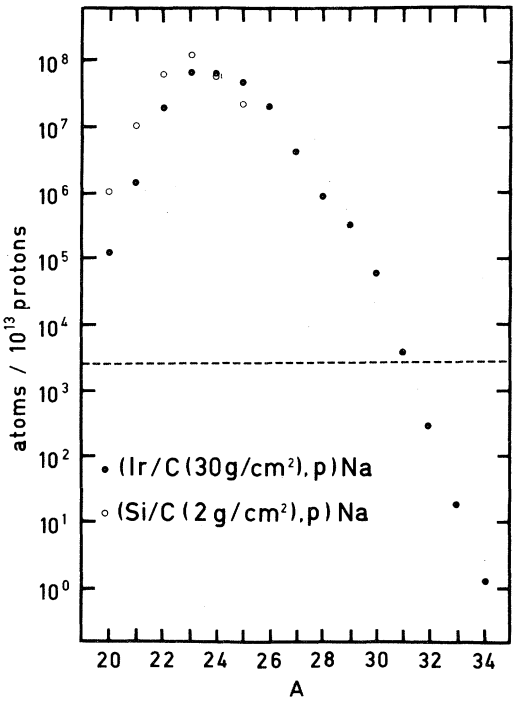

FIG. 3. Isotopic production rates of sodium isotopes. Essentially owing to the acceptance of the atomic beam apparatus, four orders of magnitude are lost between the target and the detector. The horizontal dotted line indicates our limit of sensitivity.

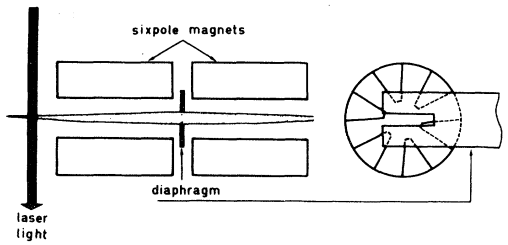

FIG. 4. Schematic view of the analyzing sixpole magnets. A movable diaphragm inserted between the two magnets increases the collimation—hence narrowing the observed resonance peaks.

contains a description of the oven used to heat the target at its normal working temperature of about 1800 °C and to produce the required thermal atomic beam.

B. Improvement of the resolution of optical resonances and of the laser frequency control

In our previous experiments,[2] the typical width of observed resonances for an atomic beam at 1500 °C was 70 MHz. This is large compared to the typical splittings in the $3p\ ^2P_{3/2}$ atomic state of sodium, namely some 50 MHz. An increase of the collimation by a factor of 2 allows separating of the resonance peaks. This has been achieved by introducing a movable diaphragm between the two sixpole magnets which compose our focusing device. This aperture is a slit 1 mm wide, perpendicular to both the atomic and the light beams (Fig. 4). Experimentally, a resonance width of 40 MHz has been obtained, while the counting rate was reduced by a factor of 3.

Since the previous experiments on the D_2 line of

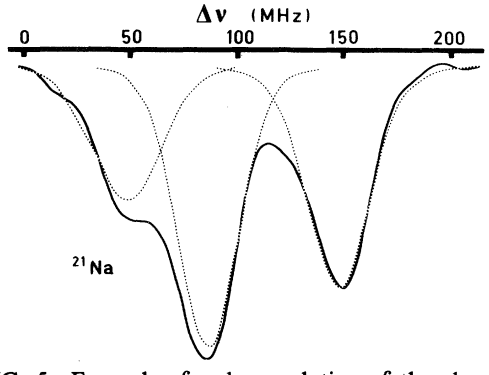

FIG. 5. Example of a deconvolution of the observed resonance peaks. The experimental curve (full line) was been smoothed before the deconvolution was performed. The dotted curves correspond to the individual resonance curves.

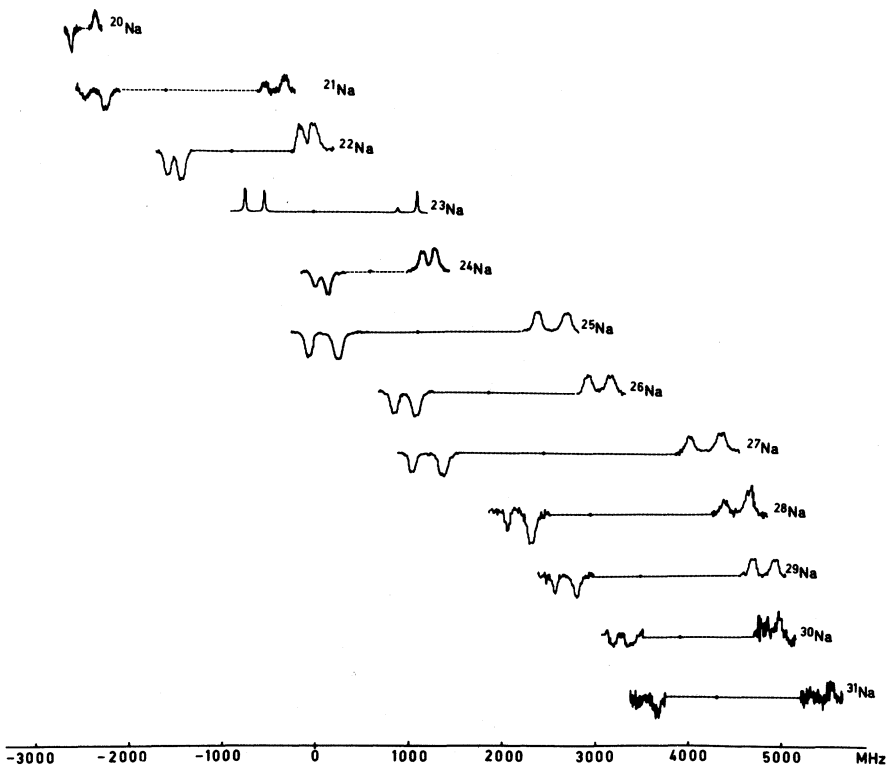

FIG. 6. Examples of observed resonance peaks in the case of the D_1 line showing their relative positions. Results obtained during a previous experiment (Ref. 2) ($^{25-30}$Na) have been included.

TABLE I. Isotope shifts of $^{21-31}$Na. The quoted errors are one standard deviation.

	$\delta\nu^{23,A}$ (MHz)	
A	This work	Other results
20	−2493.4(36)	−1800 (180)[a]
21	−1595.2(29)	−1596.7(23)[b]
22	−754.0(23)	−756.9(19)[b]
		−758.5(7)[c]
23	0	
24	705.6(18)	706.4(62)[b]
25		1347.2(13)[b]
26		1937.5(9)[b,d]
27		2481.3(20)[b]
28		2985.8(27)[b]
29		3446.2(38)[b]
30		3883.5(60)[b]
31	4282.0(35)	4286 (16)[b,d]

[a]F. C. M. Coolen and N. Van Schaick, Physica (Utrecht) 93C, 267 (1978).
[b]G. Huber *et al.* Phys. Rev. C 18, 2342 (1978).
[c]K. Pescht, H. Gerhardt, and E. Matthias, Z. Phys. A 281, 199 (1977).
[d]A printing error in the manuscript led us to publish erroneous values in Ref. b for ^{26,31}Na. The results given here should be considered as an erratum.

^{21,25}Na,[6] the laser frequency control system[10] has been improved; in particular, the long-time stability of the whole system is insured by a feed-back loop using a He-Ne laser locked on an iodine saturated absorption line.[2] This system is therefore insensitive to the room temperature and pressure drifts.

C. Detection of atoms

After being analyzed by the sixpole magnet, the alkali atoms are selectively ionized on a heated rhenium surface.[9] The ions are then mass separated[11] and counted on an electron multiplier whose first dynode is movable[12] so that the accumulated radioactivity can be removed at will. It is thus possible to reduce the background noise so that the accuracy on the measured hfs factors and IS of ^{24}Na and ^{31}Na is substantially improved (cf. Ref. 2).

D. Data processing and results

Data were stored in scalers linked via a CAMAC system to a PDP 11-34 computer. We recorded at the same time: (i) the intensity of the atomic beam,

TABLE II. $A(^2S_{1/2})$ and $A(^2P_{1/2})$ hfs factors.

		$A(^2S_{1/2})$ (MHz)			$A(^2P_{1/2})$ (MHz)	
A	I	This work	Other results		This work	Other results
20	2	110.6 (17)	110.742	(5)[a]	12.3 (17)	
21	$\frac{3}{2}$	954.1 (23)	953.7	(20)[b]	101.3 (23)	102.6 (18)[b]
			953.233	(11)[c]		
22	3	349.3 (8)	349.3	(10)[b]	37.2 (8)	37.5 (10)[b]
			348.75	(1)[d]		37.0 (1)[h]
23	$\frac{3}{2}$		885.813 064	4(5)[e]		94.25(15)[h]
24	4	253.45(15)	253.2	(27)[b]	26.95(15)	28.2 (27)[b]
			253.185 018	(23)[f]		
25	$\frac{5}{2}$		882.7	(9)[b]		94.5 (5)[b]
			882.8	(10)[g]		
26	3		569.4	(3)[b]		61.0 (3)[b]
27	$\frac{5}{2}$		933.6	(11)[b]		100.2 (11)[b]
28	1		1453.4	(29)[b]		156.0 (27)[b]
29	$\frac{3}{2}$		978.3	(30)[b]		104.4 (30)[b]
30	2		624.0	(30)[b]		66.2 (28)[b]
31	$\frac{3}{2}$	920.8 (34)	912	(15)[b]	101.7 (34)	

[a]H. Schweickert, J. Dietrich, R. Neugart, and E. W. Otten, Nucl. Phys. A246, 187 (1975).
[b]G. Huber *et al.*, Phys. Rev. C 18, 2342 (1978).
[c]O. Ames, E. A. Phillips, and S. S. Glickstein, Phys. Rev. 137, B1157 (1965).
[d]L. Davis, Jr., D. E. Nagle, and J. R. Zacharias, Phys. Rev. 76, 1068 (1949).
[e]A. Beckmann, K. D. Böklen, and D. Elke, Z. Phys. 270, 173 (1974).
[f]Y. W. Chan, V. W. Cohen, and M. Lipsicas, Phys. Rev. 150, 933 (1966); V. W. Cohen, Bull. Am. Phys. Soc. 18, 727 (1973).
[g]M. Deimling, R. Neugart, and H. Schweickert, Z. Phys. A 273, 15 (1975).
[h]K. Pescht, H. Gerhardt, and E. Matthias, Z. Phys. A 281, 199 (1977).

(ii) the step by step frequency scan of the laser (through an up-down counter), and (iii) the fluorescence signal from an auxiliary atomic beam of natural sodium, which provided the atomic frequency reference. We also recorded normalization quantities such as the proton beam intensity (cf. Ref. 2). The timing was governed by a programmable clock synchronized on the pulsed beam of the proton synchrotron.

In the cases of the D_2 line and of the ^{20}Na D_1 line, it was necessary to make a deconvolution of the unresolved resonance peaks (Fig. 5). The experimental shape has been approximated by the sum of a Gaussian and a Lorentzian curve. The validity of this assumption has been tested by studying well separated resonance peaks. Details of the procedure can be found in Refs. 13 and 14. In all cases, we have taken account of the Zeeman shifts due to the static magnetic field H_0 ($\simeq$0.9 G). The corrections due to these Zeeman shifts are always less than 1 MHz. The simultaneous recording of the fluorescence signal of the auxiliary atomic beam allows us to measure the isotope shifts relative to ^{23}Na.

The D_1 line of ^{20,21,22,24,31}Na was studied during this experiment (Fig. 6). The IS and hyperfine constants $A(^2S_{1/2})$ and $A(^2P_{1/2})$ were deduced and are given in Tables I and II.

Recordings of the $^2P_{3/2}$ atomic state hfs have been obtained for $^{21,25-27}$Na (Fig. 7). From the hfs splittings, we have determined the hyperfine constants $A(^2P_{3/2})$ and $B(^2P_{3/2})$. The results are summarized in Table III.

III. THE LASER RADIO FREQUENCY DOUBLE RESONANCE EXPERIMENT

A double resonance experiment has been performed in order to measure more accurately the $(F'=I+\frac{3}{2}, F'=I+\frac{1}{2})$ interval of the $^2P_{3/2}$ excited state of some sodium isotopes.

A. Principle of the experimental method

As mentioned above, the signal corresponding to the hyperfine component $3s\ ^2S_{1/2}$, $F=I+\frac{1}{2}\rightarrow 3p$

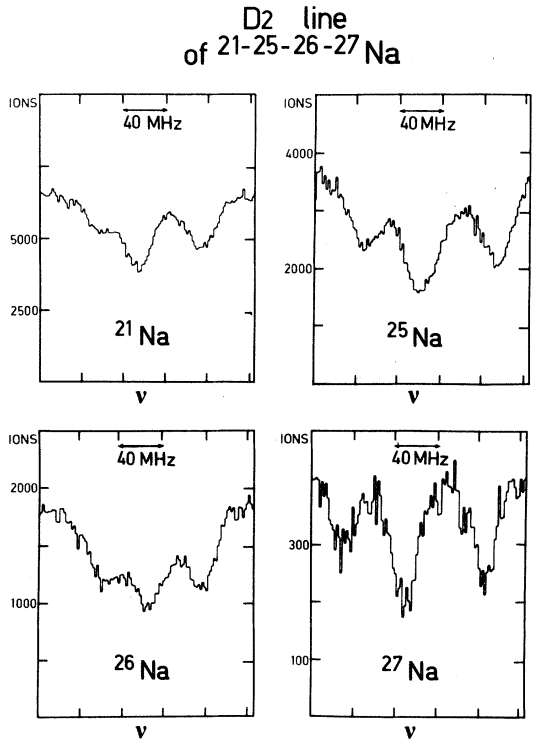

FIG. 7. Examples of observed resonance peaks in the case of the D_2 line studied by optical spectroscopy.

$^2P_{3/2}$, $F'=I+\frac{3}{2}$, i.e., the c component in Fig. 1(b) has a peculiar behavior. Since there is no hyperfine pumping for this transition, the signal is entirely due to Zeeman optical pumping. Therefore, a $\sigma^-(\sigma^+)$ polarization of the resonant light favors the lower (upper) m_F sublevel and finally produces a negative (small positive) signal on the transmitted atomic beam intensity. Moreover, for this transition, each atom can be excited several times during the transit time through the interaction region.

The laser light being σ^+ polarized and frequency tuned to resonance, one observes an increase of the transmitted atomic beam intensity (Fig. 8). Then, an rf magnetic field H_{rf} is applied in the interaction region. If its frequency ν_{rf} coincides with the frequency splitting between the two adjacent sublevels $F'=I+\frac{3}{2}$ and $F'=I+\frac{1}{2}$ of the $^2P_{3/2}$ state, a transition is induced between these two sublevels, which populates the second one. Some of the atoms transferred to this level decay by spontaneous emission to the $F=I-\frac{1}{2}$ sublevel of the ground state where they are trapped. Therefore, the detected beam intensity decreases. The whole resonance curve is obtained by scanning the radiofrequency while the laser frequency is kept at its fixed resonance value (Fig. 8). Of course, the rf field amplitude must also be kept constant all along the scan. The frequency interval of interest corresponds to the measured central frequency of the rf resonance curve. The width (FWHM) and the relative depth (S/G) of this resonance are discussed in Appendix A.

TABLE III. Hyperfine constants of the $3p\ ^2P_{3/2}$ excited states determined by optical spectroscopy.

A	$A(^2P_{3/2})$ (MHz)	$B(^2P_{3/2})$ (MHz)
21	19.2(5)	1.3(16)
25	18.6(4)	−4.6(26)
26	12.1(4)	−4.0(30)
27	20.0(4)	−4.3(31)

B. Experimental arrangement; production and measurement of the rf magnetic field

The apparatus is the same as the one used for the optical laser experiment described in Sec. II, except for some new devices which are added to generate the rf magnetic field H_{rf} and to control its amplitude. A commercial rf generator (Rohde and Schwartz SMS 0.4−1040 MHz) followed by a linear wide band amplifier (50 W, 10−250 MHz) covers the rf frequency range to be scanned.

The interaction region is schematically shown in Fig. 9. Two turns of copper rod, approximately in a Helmholtz configuration [see Fig. 9(a)] provide an rf magnetic field which is roughly homogeneous over the region where the laser beam intersects the atomic beam. This rf field is parallel to the atomic beam. The rf coil is part of a tunable tank circuit [Fig. 9(b)]. For each rf frequency, a variable capacitor is tuned until the resonance of the tank circuit is obtained, providing a strong enough rf magnetic field amplitude in the whole range 45−120 MHz.

Two Helmholtz coils (not shown in the figure) generate the static homogeneous magnetic field H_0, parallel to the laser beam. The whole interaction region is surrounded by a magnetic shield of Armco iron avoiding stray magnetic fields.

In order to keep the rf field constant during the experiment, its amplitude is detected by a single-turn pickup copper loop located near the intersection region (see Fig. 9) and connected to an rf diode and a dc voltmeter (General Radio type 874 VR). This probe is calibrated vs the frequency using a procedure described in Appendix B.

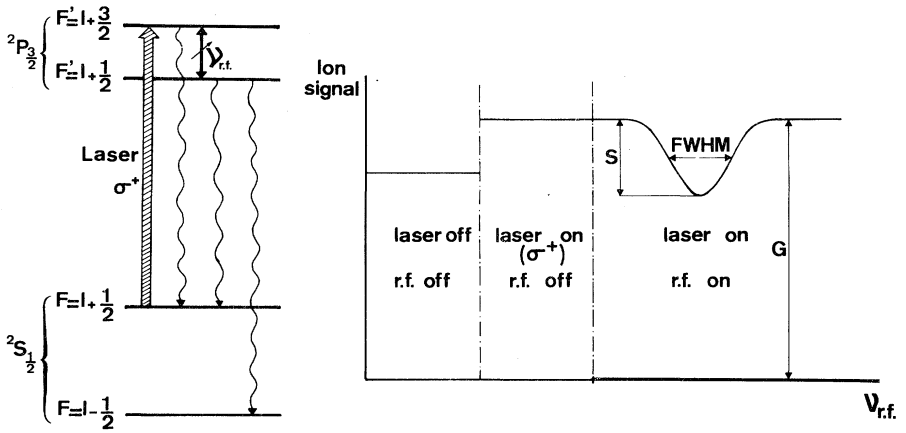

FIG. 8. Principle of the laser rf double resonance experiment. Transitions and atomic levels involved in the experiment (left); observed atomic beam intensity (right).

C. Experimental procedure and experimental results

For each step of the rf scanning, the tank circuit is tuned to maximize the signal on the pickup loop. Then, the rf magnetic field amplitude is reset to the calibrated value by adjusting the rf voltage. In order to minimize errors due to imperfect settings, the whole resonance curve is recorded several times. The different measurements are then added. Doing so, we have obtained resonance curves for six isotopes, $^{21,25-29}$Na, shown in Fig. 10.

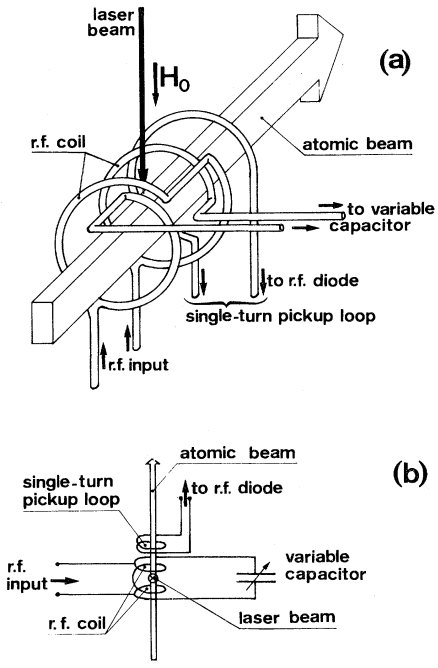

FIG. 9. Drawing in perspective (a) and schematic top view (b) of the interaction region.

For each isotope, the central frequency of the resonance ($\Delta\nu_{exp}$) is indicated in Table IV. The experimental curves exhibit a FWHM of 25–30 MHz and a relative depth (S/G) of about 20%. This width is notably larger than the expected width in a classical double-resonance experiment[7] (20 MHz). Moreover, it has been experimentally observed that any attempt to increase S/G by increasing rf or light power invariably resulted in an increase of the FWHM of the resonance curve.

In order to understand the line-shape dependence upon rf and light parameters, calculations on a four level system have been performed. They are given in Appendix A.

D. Determination of the $B(^2P_{3/2})$ hyperfine constant for $^{21,25-29}$Na

The main source of the experimental uncertainty is related to the effect on the rf resonance curve of a detuning of the laser frequency from the exact resonance. The calculations developed in Appendix A allow an estimate of this effect: A 5 MHz detuning induces a 1 MHz shift of the rf resonance curve. Since the laser can be set to a resonance better than 5 MHz, we have adopted a value of ± 1 MHz as an upper-limit error for each measured frequency interval. Only for ^{29}Na, which is the least abundant of the studied isotopes, the error has been slightly increased up to 1.2 MHz owing to statistical effects. In addition, the accuracy reached by this method of measurement has been tested in a similar experiment performed on the stable ^{23}Na isotope: The results obtained for the frequency interval ($F'=3$, $F'=2$) always differed by less than 1 MHz from the

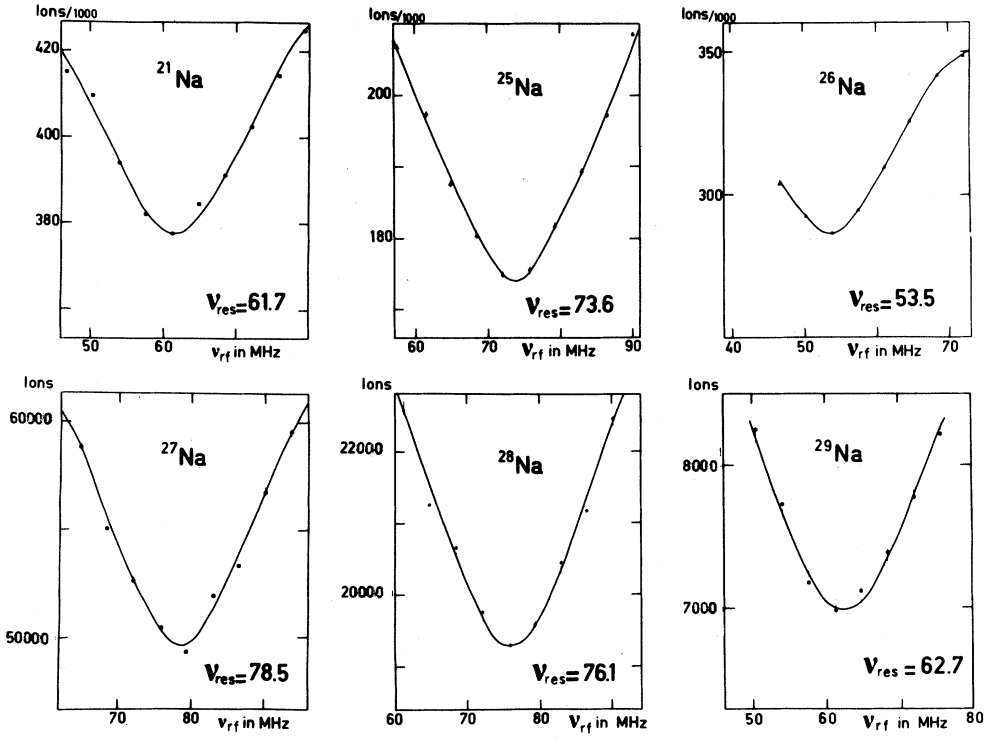

FIG. 10. Resonance curves obtained by laser rf double resonance.

value $\Delta\nu=58.77(43)$ MHz deduced from the most precise values of the hyperfine constants $A_{23}(^2P_{3/2})$ and $B_{23}(^2P_{3/2})$ quoted in the literature.[15]

We have taken into account the Zeeman shifts due to the static magnetic field ($H_0=0.9$ G) to deduce the exact values of the frequency interval $\Delta\nu_0$ ($F'=I+\frac{3}{2}$, $F'=I+\frac{1}{2}$) in zero magnetic field. Details about these corrections can be found in Ref. 13. The values of $\Delta\nu_0$ are indicated in Table IV. In all cases corrections due to the Zeeman shifts are less than 1 MHz.

Neglecting the hyperfine anomaly effects, which should be much smaller than 0.1 MHz the hyperfine constant $A_x(^2P_{3/2})$ of an isotope x can be calculated using the formula

$$A_x(^2P_{3/2})=A_{23}(^2P_{3/2})A_x(^2S_{1/2})/A_{23}(^2S_{1/2})\ .$$

For $A_{23}(^2P_{3/2})$, we used the most accurate value quoted in the literature.[15] Values of $A_{23}(^2S_{1/2})$ and $A_x(^2S_{1/2})$ are indicated in Table II. The calculated values of $A_x(^2P_{3/2})$ are reported in Table IV. The $B(^2P_{3/2})$ hyperfine constant is then obtained, for

TABLE IV. Hyperfine constant $B(^2P_{3/2})$ determined by laser rf double resonance spectroscopy.

A	$\Delta\nu_{exp}$ (MHz) $H_0=0.9$ G	$\Delta\nu_0$ (MHz) ($H_0=0$) $F'=I+\frac{3}{2}\leftrightarrow F'=I+\frac{1}{2}$	$A(^2P_{3/2})$ (MHz) Calculated	$B(^2P_{3/2})$ (MHz)
21	61.7(10)	61.4(10)	20.07(12)	1.2(11)
25	73.6(10)	73.1(10)	18.58(10)	−1.6(14)
26	53.5(10)	52.9(10)	12.00(7)	−1.5(14)
27	78.5(10)	78.0(10)	19.65(11)	−0.8(14)
28	76.1(10)	75.9(10)	30.60(18)	−0.4(9)
29	62.7(12)	62.4(12)	20.60(13)	0.6(13)

TABLE V. Spectroscopic quadrupole moment of the sodium isotopes.

A	$B(^2P_{3/2})$ (MHz)	Q_s (b)
21	1.2(9)[a]	0.050(37)
25	−2.3(12)[a]	−0.095(50)
26	−1.9(13)[a]	−0.079(54)
27	−1.4(13)[a]	−0.058(54)
28	−0.4(9)	−0.017(37)
29	0.6(13)	0.025(54)

[a]Weighted average of the results obtained by optical spectroscopy (Table III) and by laser rf double resonance spectroscopy (Table IV).

each isotope, through the formula

$$B(^2P_{3/2})=2I\left[\frac{\Delta\nu_0}{I+3/2}-A(^2P_{3/2})\right].$$

The results are given in Table IV. They are approximately twice as accurate as those obtained by laser optical spectroscopy and are in agreement with them (see Table III).

IV. DISCUSSION

A. Quadrupole moments

The spectroscopic quadrupole moment can be deduced from the hfs $B(^2P_{3/2})$ factor. For this purpose, Hartree-Slater calculations[16] have been used, as they also provide the best agreement with measured magnetic moments. Therefore, we have

$$Q_s=4.134\ 10^{-2}B(^2P_{3/2})$$

where Q_s is in b and $B(^2P_{3/2})$ in MHz. We have used the weighted average of the $B(^2P_{3/2})$ factors measured by optical and double-resonance experiments. Results are given in Table V.

The sign of the quadrupole moment seems to indicate an oblate deformation for $^{25-28}$Na and a prolate deformation for other studied isotopes. This does not contradict the conclusions we had drawn from magnetic moments discussed within the framework of the Nilsson model.[2,17] Because of the very low counting rate, no recording of ^{31}Na was obtained so that we cannot make any conclusion concerning the deformation region at $N=20$. An evaluation of the deformation parameter $\langle\beta\rangle$ can be derived from the intrinsic quadrupole moment Q_0 which is related to the spectroscopic quadrupole moment via the well-known formula:

$$Q_s=Q_0[I(2I-1)]/[(I+1)(2I+3)],$$

which has been established within the framework of the collective model. $\langle\beta\rangle$ is calculated using

$$Q_0=\frac{3}{\sqrt{5\pi}}ZR_0^2\langle\beta\rangle\left[1+\frac{1}{8}\left[\frac{5}{\pi}\right]^{1/2}\langle\beta\rangle\right]$$

with $R_0=r_0A^{1/3}$, where $r_0=1.2$ fm. Results are given in Fig. 11, together with values of $\langle\beta^2\rangle^{1/2}$ of some neon and magnesium isotones deduced from $B(E2)$ measurements, Coulomb excitation, or proton inelastic scattering.[18,19] It can be noticed that in all cases, $\langle\beta^2\rangle^{1/2}$ is indeed larger than $|\langle\beta\rangle|$. This expresses that the quadrupole moment takes into account only static deformations while other results, leading to $\langle\beta^2\rangle$, are also sensitive to zero point vibrations.

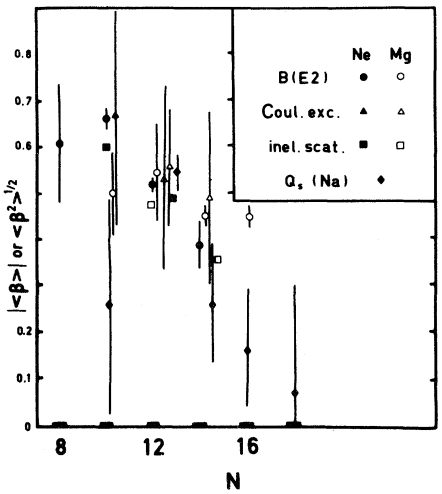

FIG. 11. Experimental deformation parameter of neon, sodium, and magnesium isotopes. Results coming from $B(E2)$ determinations, Coulomb excitation or inelastic scattering lead to $\langle\beta^2\rangle^{1/2}$. They have been taken from Refs. 18 and 19. Electric quadrupole moments lead to $\langle\beta\rangle$ (here $|\langle\beta\rangle|$ is shown).

Recently, Möller and Nix[20] have computed the deformations of the ground state of nuclei using a macroscopic-microscopic model. The energy is minimized as a function of the deformation parameters β_2 (quadrupole deformations) and β_4 (hexadecapole deformations). In the case of sodium, quadrupole deformations are dominant. A sudden change in the quadrupole moment, and therefore in the deformation, is indeed predicted to occur at $N=20$ for both sodium and magnesium isotopes. A comparison of the experimental and theoretical deformation parameters $\langle\beta\rangle$ is given in Fig. 12. The

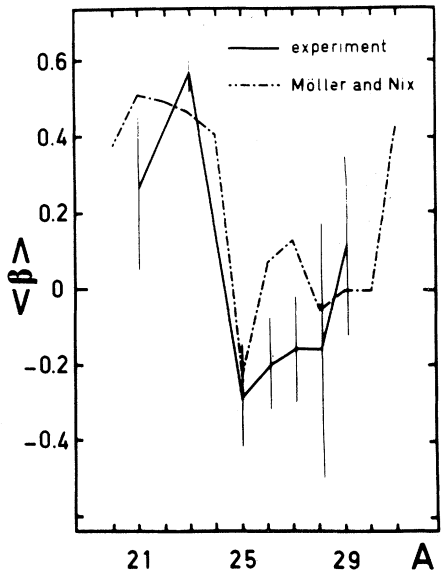

FIG. 12. Comparison of the experimental nuclear quadrupole deformation and calculated deformation by Möller and Nix (Ref. 20).

general agreement is good; in particular, the negative sign of the quadrupole moment of ^{25}Na is well reproduced.

B. Isotope shift

In Ref. 2, the existence of a volume effect in the isotope shift of the sodium isotopes was established. The isotope shift can be expressed as

$$\delta\nu^{A,A'}=\delta\nu^{A,A'}_{\text{mass}}+\delta\nu^{A,A'}_{\text{volume}} .$$

The mass effect is dominant for light elements, and is given by

$$\delta\nu^{A,A'}_{\text{mass}}=(K_{\text{nms}}+K_{\text{sms}})\left[\frac{1}{M_A}-\frac{1}{M_{A'}}\right] .$$

K_{nms} and K_{sms} correspond, respectively, to the normal (Bohr) mass effect and to the specific mass effect. The latter describes the mutual interaction of the orbital electrons and cannot be calculated with a good accuracy.

The volume effect is linked to the change in the mean square charge radius by (cf. Ref. 21)

$$\delta\nu^{A,A'}_{\text{volume}}=F\delta\langle r^2\rangle^{A,A'}$$
$$=F[\langle r^2\rangle^{A'}-\langle r^2\rangle^{A}] ,$$

where F is an electronic constant of the element.

As there is only one stable sodium isotope, no absolute measurement of $\delta\langle r^2\rangle$ has been performed, and therefore experimental determination of F and K_{sms} is impossible. F has been calculated following the procedure described in Ref. 21. We obtain $F=-47$ MHz/fm^2.

In order to determine K_{sms}, we have evaluated $\delta\langle r^2\rangle^{25,27}$ from a semiempirical point of view: $\delta\langle r^2\rangle$ can be written as the sum of two terms, one describing the behavior of a sphere to which neutrons are added, the other one taking into account the effect of the deformation (see e.g., Refs. 8, 22, or 23):

$$\delta\langle r^2\rangle=\delta_{\text{sph}}\langle r^2\rangle+\delta_\beta\langle r^2\rangle$$
$$=\delta_{\text{sph}}\langle r^2\rangle+\frac{5}{4\pi}\delta[\langle\beta^2\rangle\langle r^2\rangle_{\text{sph}}] . \quad (1)$$

$\langle r^2\rangle_{\text{sph}}$ has been approximated by the well-known expression $\langle r^2\rangle_{\text{std}}=\frac{3}{5}(r_0A^{1/3})^2$, where $r_0=1.2$ fm. $\langle\beta^2\rangle$ has been estimated from the comparison of results concerning neon and magnesium isotones (cf. Fig. 11) (results from our Q_s measurements would underestimate the deformation, since zero-point vibration would not be taken into account). $\delta_{\text{sph}}\langle r^2\rangle^{25,27}$ could be estimated using the so-called "standard law"

$$\delta_{\text{sph}}\langle r^2\rangle=\zeta\delta\langle r^2\rangle_{\text{std}}$$
$$=\zeta\tfrac{2}{5}r_0^2A^{-1/3}\delta A .$$

ζ is an empirical correction factor, the "isotope shift discrepancy," which is generally found to be around 0.5 all over the valley of β stability. Hartree-Fock calculations,[4] which predict a very small change in the deformation between ^{25}Na and ^{27}Na, can be fitted in this region by the standard law with $\zeta=0.5$. Taking this value for the isotope shift discrepancy, it is now straightforward to calculate $K_m=K_{\text{nms}}+K_{\text{sms}}$. We find $K_m\simeq385$ GHz u. The evaluation of $\delta\langle r^2\rangle$ for all other isotopes can then be derived. Results are given in Fig. 13. Dashed and dotted lines correspond to an error of $\pm10\%$ on the deformation parameter of ^{25}Na and ^{27}Na, all other souces of error being omitted.

In Fig. 14, we compare the measured changes in the mean-square charge radius, with $K_m=385.5$ GHz u, with the ones calculated by Campi *et al.*[4] Agreement between experiment and calculations is rather good for nuclei with $A<27$ while the expected bump at $A=31$ is not observed. The first point can be considered as new evidence for the static deformation around ^{23}Na. To our knowledge, no obvious interpretation of the discrepancy beginning at $A=28$ is available. A possible assumption could be that large zero-point surface vibrations may occur

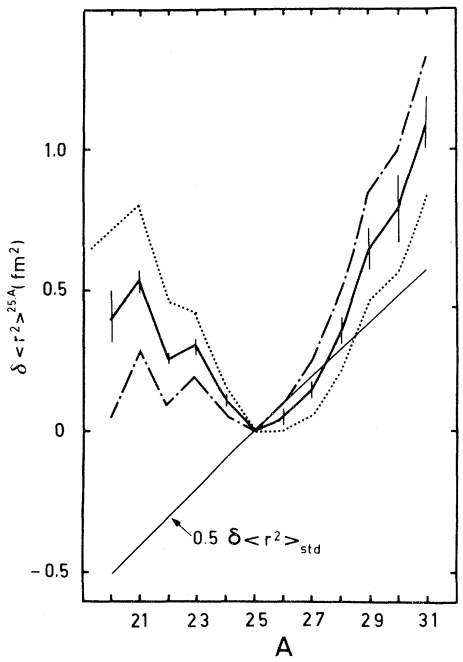

FIG. 13. Estimation of the variation of the mean-square nuclear charge radius of sodium isotopes using $K_m = 385$ GHz u. Dashed and dotted lines correspond to variations of $\pm 10\%$ for $\beta(25, 27)$ (see text for details).

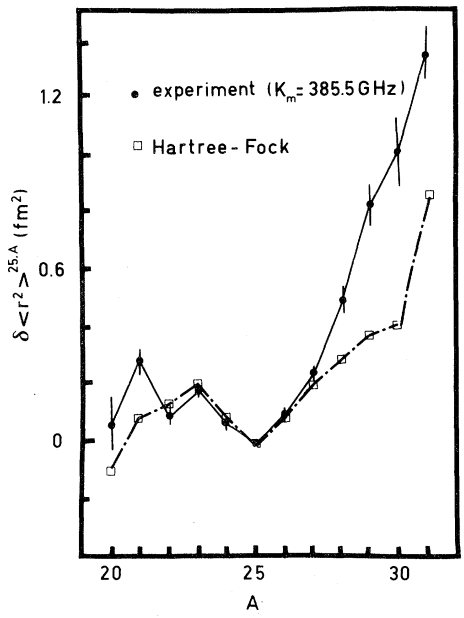

FIG. 14. Comparison of experimental and calculated (Ref. 4) values of $\delta\langle r^2\rangle$. K_m has been chosen so that the agreement of $\delta\langle r^2\rangle^{25,A}$ is as good as possible for $A=23$, 27.

for nuclei heavier than ^{28}Na and consequently would hide the static deformation at $N=20$.

We point out a strong shell effect arising at $N=14$ ($A=25$), corresponding to the closure of the $d_{5/2}$ subshell. It becomes evident when the spherical part of $\delta\langle r^2\rangle$ is expressed following the standard law

$$\delta_{\text{sph}}\langle r^2\rangle = \zeta \delta\langle r^2\rangle_{\text{std}} .$$

When $\delta_\beta\langle r^2\rangle$ has been evaluated it is possible to derive $\delta_{\text{sph}}\langle r^2\rangle$ from our measurements by means of relation (1); ζ is then extracted by comparing $\delta\langle r^2\rangle_{\text{std}}$ and $\delta_{\text{sph}}\langle r^2\rangle$. $\zeta(A)$ has been evaluated for sodium isotopes for which an average of measured $\langle\beta^2\rangle$ of neon and magnesium isotopes is available. We find $\zeta(27)=0.5$, as expected, since it is one of our assumptions, but $\zeta(23)\simeq -0.3$ and $\zeta(21)\simeq -0.3$. Of course, uncertainties are very large ($\simeq 0.3$). But, whatever the assumptions, $\zeta(21)$ and $\zeta(23)$ on one hand and $\zeta(27)$ on the other, are never compatible. It seems very likely that the spherical part of the nucleus decreases when neutrons are added in the $d_{5/2}$ subshell and increases when the $s_{1/2}$ subshell is filled. We had already observed the same kind of effect for heavier elements.[8,24] Nolen and Schiffer[25] have discussed a similar behavior in the case of calcium isotopes. It can be interpreted in terms of a competition between the nuclear potential (shell dependent) which causes a shrinking of the nuclear core and the increase of the nuclear volume, both occurring when neutrons are added.

V. CONCLUSION

On-line Doppler-free laser spectroscopy on a thermal atomic beam has allowed us to study the isotope shifts of $^{20-31}$Na. Using a double resonance technique, we have been able to study the hyperfine structure of the $3p\ ^2P_{3/2}$ excited state of $^{21,25-29}$Na.

We have deduced the quadrupole moments and the changes in the mean-square charge radius of these isotopes. There is no evidence of the sudden onset of the strong deformation appearing at $N=20$ predicted by Hartree-Fock or macroscopic-microscopic calculations. However, since it was not possible to measure the quadrupole moment of ^{31}Na, no definite conclusion can be drawn.

A strong shell effect in the spherical part of the charge radius occurs at $N=14$. When neutrons are added, the spherical radius decreases up to ^{25}Na; above ^{25}Na, it increases as would be expected. New measurements of quadrupole moments and charge radii in that region by both atomic and nuclear spectroscopy would be highly valuable.

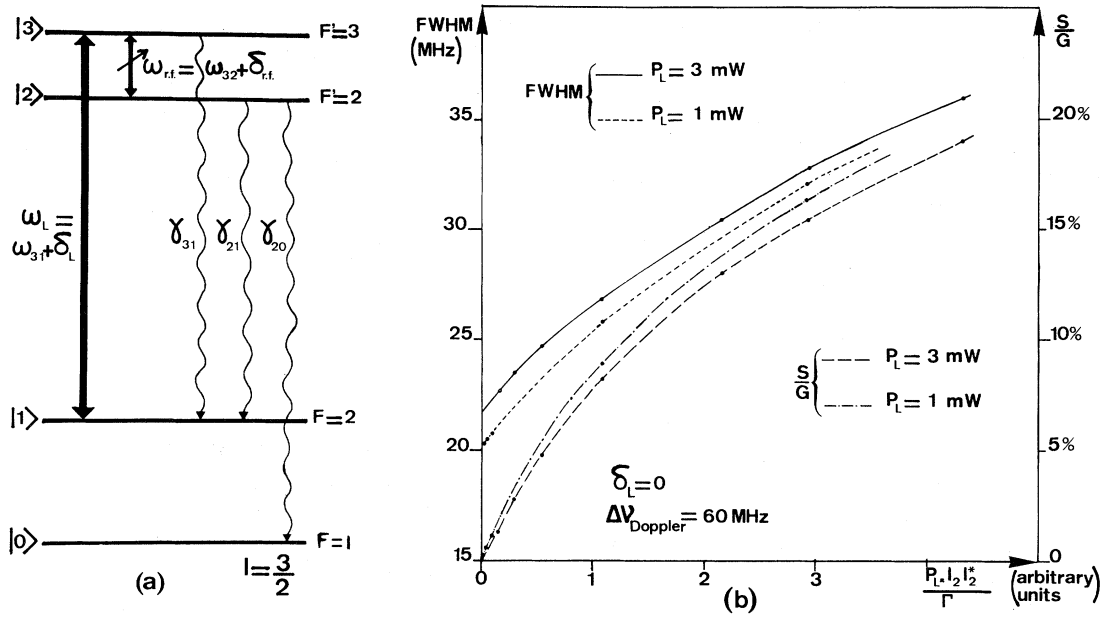

FIG. 15. (a) Energy-level diagram of the theoretical four level system and characteristics of the two oscillating fields. (b) Results of the calculations. The laser field is exactly resonant; the relative depth (S/G) and the width (FWHM) of the rf resonance are plotted as functions of $p=P_L I_2 \cdot I_2^*/\Gamma$ (see text).

ACKNOWLEDGMENTS

We express our special gratitude to Prof. G. Huber and Prof. P. Jacquinot who took a very large part in the initiation of this work. It is a pleasure to acknowledge the able assistance of R. Baronnet, J. Biderman, R. Fergeau, J. F. Képinski, M. Jacotin, G. Le Scornet, C. Vialle, and the CERN proton synchrotron technical staff before and during the experiments. One of us (S.B.) would thank the Deutsche Forschungsgemeinschaft for a fellowship.

APPENDIX A: CALCULATION OF THE WIDTH AND DEPTH OF THE RF RESONANCE CURVE. EFFECT OF A SLIGHT LASER DETUNING

A. The four level system

We consider a four level system $|0\rangle$, $|1\rangle$, $|2\rangle$, $|3\rangle$ [see Fig. 15(a)] corresponding to the two hyperfine sublevels of the ground state and the two hyperfine sublevels of the $3p\ ^2P_{3/2}$ excited state involved in our experiment. The spontaneous emission transition probabilties γ_{ij} are also indicated in the figure. The calculation is carried out for the particular case of a nuclear spin $I=\frac{3}{2}$. The atomic system is coupled with two oscillating fields: an optical field, whose frequency ω_L is fixed and resonant or quasiresonant with the atomic frequency ω_{31} ($\omega_L=\omega_{31}+\delta_L$), and an rf field whose frequency $\omega_{\rm rf}$ is scanned on both sides of the atomic frequency ω_{32} ($\omega_{\rm rf}=\omega_{32}+\delta_{\rm rf}$).

In a first calculation, we assume that the laser is exactly resonant ($\delta_L=0$) and we calculate the signal, i.e., the change in the population of the state $|1\rangle$ as a function of the rf detuning $\delta_{\rm rf}/2\pi$. The relative depth (S/G) and the frequency width (FWHM) of this calculated resonance curve are analyzed in terms of three parameters: the interaction time, the laser field strength, and the rf field strength.

In a second step, these parameters are chosen so that the depth and the frequency width of the calculated resonance curve correspond to the experimental situation and the laser frequency is detuned ($\delta_L\neq 0$). The central frequency of the rf resonance curve is then studied as a function of the laser detuning $\delta_L/2\pi$.

B. The calculation procedure

Many papers have treated atomic systems (generally three level systems) interacting with two quasiresonant monochromatic fields (see e.g., Refs. 26, 27, 28, and 29). We have adapted to our particular case the theoretical treatment developed, for in-

stance, in Refs. 26 and 27. Therefore, we shall discuss here only the most important and the results.

When the rf is turned off, the optical Zeeman pumping tends to populate the $F=2$, $m_F=2$ substate of the ground state and the $F'=3$, $m_{F'}=3$ substate of the excited state. When the rf is turned on, we assume that the situation is nearly the same, i.e., the effect of the rf field on the atomic system is much weaker than that of the optical field. Therefore, the four levels of our theoretical model can be considered as nondegenerate levels, thus avoiding Zeeman degeneracy effects.[27]

As in Refs. 26 and 27, the semiclassical approximation is adopted: The atomic system is treated quantum mechanically, using the density matrix formalism, while the fields are treated classically. One has also to deal with Doppler effect in the same way as in Ref. 26. It is, of course, negligible for the rf transitions while for the optical resonances, the Doppler width is about 60 MHz.

The rate equation of the density operator ρ_v corresponding to a given velocity class is

$$\frac{d}{dt}\rho_v=\frac{-i}{\hbar}[\mathscr{H},\rho_v]+\Lambda+\left[\frac{d\rho_v}{dt}\right]_{\text{relax}}. \tag{2}$$

$\mathscr{H}$ represents the atomic Hamiltonian and the coupling interaction with the two fields. Λ describes the atomic populations traveling into the interaction region. $(d\rho_v/dt)_{\text{relax}}$ describes the relaxation phenomena: It has a term due to spontaneous emission and a phenomenological term $-\Gamma\times\rho_v$ which takes into account the finite interaction time and therefore the atoms traveling out of the interaction region.[30] Since the interaction time $\tau=1/\Gamma$ is of the order of 10^{-5} s in our experimental case, we have, therefore, $\Gamma\ll\gamma_{31}, \gamma_{21}, \gamma_{20}$.

For each velocity class, the stationary solution $\bar{\rho}_v$ of Eq. (2) is obtained using the rotating wave approximation. One has to integrate this result over the velocity distribution,

$$\bar{\rho}=\int \bar{\rho}_v N(v)\,dv\ , \tag{3}$$

as explained in Ref. 26.

The strength of the coupling of the atomic system with each field is characterized by a Rabi nutation frequency

$$\Omega_L=2I_L=\hbar^{-1}\langle 1\,|\,\vec{\mathrm{E}}_L\cdot\vec{\mathrm{D}}\,|\,3\rangle$$

for the laser field and

$$\Omega_{\text{rf}}=2I_2=\hbar^{-1}\langle 3\,|\,\vec{\mathrm{H}}_{\text{rf}}\cdot\vec{\mu}\,|\,2\rangle$$

for the rf field. The solution of Eqs. (2) and (3) depends on three independent parameters, $I_L\cdot I_L^*$, $I_2\cdot I_2^*$, respectively proportional to the laser energy density and the rf energy density, and Γ. If we assume that the atomic transition induced by the laser excitation is the transition ($F=2$, $m_F=2\rightarrow F'=3$, $m_{F'}=3$) and if the cross section of the laser beam is known, $I_L\cdot I_L^*$ can be precisely related to the laser power P_L at the atomic beam. We found I_L [MHz]$=8.8\sqrt{P_L}$ [mW] and in our experimental case, P_L lies between 1 and 3 mW.

C. Results

In a first step, as explained above, the laser frequency is resonant ($\delta_L=0$), and we calculate the relative depth (S/G) and the width (FWHM) of the rf resonance curve for different sets of the adjustable parameters Γ, $I_2\cdot I_2^*$, and P_L.

At first, when Γ and $I_2\cdot I_2^*$ are changed so that $I_2\cdot I_2^*/\Gamma$ is kept constant, the depth and the width are not modified. The good parameter is then $I_2\cdot I_2^*/\Gamma$. Of course this is valid only if the rf power is well below the saturation limit ($I_2\cdot I_2^*\ll\gamma_{ij}^2$).

The results obtained for the depth (S/G) and the width (FWHM) of the rf resonance curve for the two extreme cases $P_L=1$ mW and $P_L=3$ mW are displayed in Fig. 15(b). It appears that each of these two quantities may be expressed as a function of single parameter $p=P_L I_2\cdot I_2^*/\Gamma$. The slight difference between the curves corresponding to $P_L=1$ mW and $P_L=3$ mW is probably due to a weak saturation and power broadening for the laser-induced transition: for $P_L=3$ mW, one has $\Omega_L=2I_L\simeq 31\times 10^6$ s^{-1} which is not much smaller than $\gamma_{31}=63\times 10^6$ s^{-1}.

Two important remarks must be pointed out:

(i) Both the depth and the width of the resonance curve increase with p, and it is therefore impossible to get a large signal and a resonance width of the order of the lower limit width (20 MHz).

(ii) This broadening of the resonance curve is not a power broadening but is due to optical pumping, since it can be observed also at low fields powers by increasing the interaction time $1/\Gamma$.

Comparison of the theory and experiment is reasonably good: If we assume $P_L=1$ mW, our theoretical model gives $S/G=17\%$ and FWHM $=32$ MHz for a given value P_0 of the parameter p, while the corresponding experimental quantities are, respectively, of the order of 20% and 25–30 MHz.

For the second step of the calculation, the parameters P_L, $I_2\cdot I_2^*$, and Γ are kept at fixed values, and

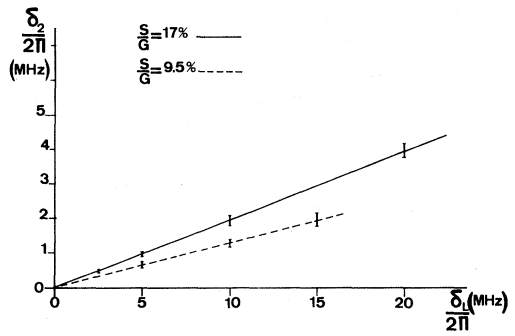

FIG. 16. Results of the calculations. The laser field is detuning from the exact atomic resonance; the frequency shift of the center of the rf resonance is plotted versus the laser detuning for two particular values of S/G. The experimental situation corresponds approximately to the case $S/G=17\%$.

the rf resonance curve is studied as a function of the laser detuning $\delta_L/2\pi$. One finds that the rf resonance curve becomes weakly asymmetric and is slightly frequency shifted when the laser is detuned. The frequency shift $\delta_2/2\pi$ of the center of the rf resonance curve is plotted versus $\delta_L/2\pi$. Results are presented in Fig. 16 for the two values of the parameter p corresponding to $S/G=17\%$ and 9.5%; $\delta_2/2\pi$ is approximately proportional to $\delta_L/2\pi$. In our experimental situation ($S/G\simeq 20\%$) we have adopted

$$\delta_2/2\pi=0.2\delta_L/2\pi \quad (4) .$$

This frequency shift of the rf resonance curve due to a laser detuning has been experimentally observed; these observations confirm the sign and the order of magnitude of this effect.

APPENDIX B: CALIBRATION OF THE PICKUP LOOP RESPONSE VERSUS RF FREQUENCY

This calibration has been obtained by performing a preliminary double resonance experiment, with the same apparatus, on a ^{138}Ba atomic beam. This atomic beam interacts with the light beam of a single-mode tunable dye laser. In this experiment, the laser beam is perpendicular to both the atomic beam and the static magnetic field H_0, its polarization is parallel to H_0 (π polarization) and its frequency is resonant with the BaI resonance line $6s^2\,{}^1S_0 \rightarrow 6s\,6p\,{}^1P_1$ at $\lambda=553.5$ nm. Owing to the choice of the polarization of the laser field, only the π component ($\Delta m_J=0$) of the normal Zeeman triplet of this line is excited. The frequency of this component is insensitive to the amplitude of H_0. The π-polarized fluorescence light, emitted in the direction of the atomic beam, is detected by a photomultiplier. A feedback loop locks the laser frequency onto the π component of the atomic transition. A second photomultiplier detects the σ-polarized fluorescence light emitted in the H_0 direction. Without the rf field, there is no fluorescent signal on this second photomultiplier, but, when the rf field is applied and its frequency corresponds to the Zeeman splitting of the excited state, rf transitions are induced in the excited state ($\Delta m_J=\pm 1$) and σ fluorescent light is observed. Since the Zeeman effect is linear, the rf resonance curve is easily scanned by sweeping the static magnetic field H_0 while the rf frequency is kept constant. With the rf powers used here, one can verify that for a given rf frequency, the σ fluorescent signal is proportional to the square of the output voltage of the rf generator and therefore to the square of the rf magnetic field amplitude, indicating that saturation effects are avoided.

A set of rf frequencies covering the frequency range of interest (45–120 MHz) is chosen. For each rf frequency, the tank circuit is tuned to resonance by varying the tunable capacitor until the rf magnetic field amplitude, as measured with the pickup loop and the diode, is maximized. Then the static field H_0 is scanned and the rf resonance curve is observed on the σ fluorescent light. H_0 is set at its resonant value and, by changing the rf output voltage of the rf generator, the σ fluorescent signal is brought back to a fixed value, the same for all the frequencies of the chosen set. The corresponding voltage on the rf diode is read, giving an experimental point of the needed calibration curve. Finally, the calibration curve of the rf pickup loop is interpolated using the points obtained for the set of frequencies.

---

*Permanent address: Institut für Angewandte Physik, Universität Bonn, D-5300 Bonn, Germany.
†Present address: DG Division, CERN, Ch. 1211 Genève 23, Switzerland.
‡Laboratoire associé à l'Université Paris-Sud.

[1]G. Huber, C. Thibault, R. Klapisch, H. T. Duong, J. L. Vialle, J. Pinard, and P. Jacquinot, Phys. Rev. Lett. 34, 1209 (1975).
[2]G. Huber, F. Touchard, S. Büttgenbach, C. Thibault, R. Klapisch, H. T. Duong, S. Liberman, J. Pinard, J. L. Vialle, P. Juncar, and P. Jacquinot, Phys. Rev. C 18, 2342 (1978).

[3]C. Thibault, R. Klapisch, C. Rigaud, A. M. Poskanzer, R. Prieels, L. Lessard, and W. Reisdorf, Phys. Rev. C 12, 644 (1975).
[4]X. Campi, H. Flocard, A. K. Kerman, and S. Koonin, Nucl. Phys. A151, 193 (1975).
[5]C. Détraz, D. Guillemaud, G. Huber, R. Klapisch, M. Langevin, F. Naulin, C. Thibault, L. C. Carraz, and F. Touchard, Phys. Rev. C 19, 164 (1979).
[6]G. Huber, R. Klapisch, C. Thibault, H. T. Duong, P. Juncar, S. Liberman, J. Pinard, J. L. Vialle, and P. Jacquinot, C. R. Acad. Sci. Paris 282, B119 (1976).
[7]M. L. Perl, I. I. Rabi, and B. Senitzky, Phys. Rev. 98, 611 (1955).
[8]C. Thibault, F. Touchard, S. Büttgenbach, R. Klapisch, M. de Saint Simon, H. T. Duong, P. Jacquinot, P. Juncar, S. Liberman, P. Pillet, J. Pinard, J. L. Vialle, A. Pesnelle, and G. Huber, Phys. Rev. C 23, 2720 (1981).
[9]F. Touchard, J. Biderman, M. de Saint Simon, C. Thibault, G. Huber, M. Epherre, and R. Klapisch, Nucl. Instrum. Methods 186, 329 (1981).
[10]P. Juncar and J. Pinard, Opt. Commun. 14, 438 (1975).
[11]M. de Saint Simon, M. Langevin, R. Fergeau, D. Guillemaud, M. Jacotin, J. F. Kepinski, R. Klapisch, C. Thibault, and F. Touchard, Nucl. Instrum. Methods 186, 87 (1981).
[12]F. Touchard, G. Huber, R. Fergeau, C. Thibault, and R. Klapisch, Nucl. Instrum. Methods 155, 449 (1978).
[13]J. M. Serre, Thèse de 3ème cycle, Orsay, 1981 (unpublished).
[14]P. Guimbal, Thèse de 3ème cycle, Orsay, 1981 (unpublished).
[15]G. H. Fuller, J. Phys. Chem. Ref. Data 5, 835 (1976).
[16]A. Rosén and I. Lindgren, Phys. Scr. 6, 109 (1972).
[17]F. Touchard, Ph.D. thesis, Orsay, 1981 (unpublished).
[18]E. Fabricci, S. Micheletti, M. Pignanelli, F. Resmini, R. de Leo, G. d'Erasmo, and A. Pantaleo, Phys. Rev. C 21, 844 (1980).
[19]*Table of Isotopes,* 7th ed., edited by C. M. Lederer and V. S. Shirley (Wiley, New York, 1978).
[20]P. Möller and J. R. Nix, Los Alamos Report LA-UR 80-1996, 1980.
[21]K. Heilig and A. Steudel, At. Data. Nucl. Data Tables 14, 613 (1974).
[22]C. Thibault, F. Touchard, S. Büttgenbach, R. Klapisch, M. de Saint Simon, H. T. Duong, P. Jacquinot, P. Juncar, S. Liberman, P. Pillet, J. Pinard, J. L. Vialle, A. Pesnelle, and G. Huber, Nucl. Phys. A367, 1 (1981).
[23]P. Jacquinot and R. Klapisch, Rep. Prog. Phys. 42, 773 (1979).
[24]F. Touchard, P. Guimbal, S. Büttgenbach, R. Klapisch, M. de Saint Simon, J. M. Serre, C. Thibault, H. T. Duong, P. Juncar, S. Liberman, J. Pinard, and J. L. Vialle, Phys. Lett. 108B, 169 (1982).
[25]J. P. Nolen and J. A. Schiffer, Annu. Rev. Nucl. Sci. 19, 471 (1969).
[26]S. Feneuille and M. G. Schweighofer, J. Phys. 36, 781 (1975).
[27]C. Delsart and J. C. Keller, J. Phys. B 13, 241 (1980).
[28]T. Hänsch and P. Toschek, Z. Phys. 236, 213 (1970).
[29]M. S. Feld and A. Javan, Phys. Rev. 177, 540 (1969).
[30]J. L. Vialle, Ph.D. thesis, Orsay, 1980 (unpublished).